Received: 8 May 2025 | Revised: 4 September 2025 | Accepted: 10 September 2025

DOI: 10.1002/btpr.70080

BIOTECHNOLOGY PROGRESS

RESEARCH ARTICLE

Cell Culture and Tissue Engineering

Dynamic pH profiles drive higher cell-specific and volumetric productivity

Stephanie R. Klaubert[1] | Dylan G. Chitwood[2] | Danqia Peng[3] | Erin Redman[4] | Ji Young L. Anderson[5] | Nicholas R. Sandoval[3] | Sarah W. Harcum[2]

[1]Department of Chemical and Biomolecular Engineering, Clemson University, Clemson, South Carolina, USA

[2]Department of Bioengineering, Clemson University, Clemson, South Carolina, USA

[3]Department of Chemical and Biomolecular Engineering, Tulane University, New Orleans, Louisiana, USA

[4]Department of Research and Development, 908 Devices, Inc., Morrisville, North Carolina, USA

[5]Department of Research and Development, 908 Devices, Inc., Boston, Massachusetts, USA

Correspondence
Stephanie R. Klaubert, Department of Chemical and Biomolecular Engineering, Clemson University, Clemson, SC 29634, USA.
Email: sklaubert27@gmail.com

Funding information
National Science Foundation, Grant/Award Number: OIA-1736123

Abstract

Mammalian cell cultures in bioreactors rely heavily on critical process parameter control to ensure optimal growth, productivity, and reproducibility to produce recombinant therapeutic proteins. Culture pH has been shown to be a critical parameter that influences growth, productivity, and critical quality attributes. Typically, pH is either controlled to a set-point throughout the culture or uses a single pH shift to achieve higher productivity and more desirable charge variant profiles. The pH is usually maintained by CO_2 and base additions. For CO_2 controlled cultures, using a set-point can result in an accumulation of CO_2, which has detrimental effects on mammalian cell growth and protein production. In this study, a dynamic pH profile was implemented that allowed the pH control in the bioreactor to mimic the natural uncontrolled pH profile observed in shake flask cultures. This dynamic pH profile employs multiple pH shifts during the exponential phase of a single IgG_1 producing CHO-K1 cell line. The results show that a dynamic pH profile was able to successfully alleviate CO_2 accumulation and increase the cell-specific, as well as overall culture productivity. Impacts of the dynamic pH profile on product quality attributes, including glycosylation and charge variants, were also evaluated, showing mixed impacts on the glycosylation pattern and a positive impact on charge variants. Since the ideal glycosylation pattern is highly dependent on the intended function of the recombinant antibody, impacts on product quality should be evaluated on a "per process" basis.

KEYWORDS
CHO, CO_2 accumulation, fed-batch, pH control, product quality, productivity

1 | INTRODUCTION

Chinese hamster ovary (CHO) cells continue to be a successful platform to produce recombinant protein-based therapeutics due to the cells' ability to perform post-translational modifications analogous to human proteins.[1,2] Since CHO cell proteins occupy a large portion of the pharmaceutical market,[3] optimizing CHO cell processes is a major research concern. Process tuning typically involves optimization of basal media and feed compositions, process parameters, and feeding strategies.[1,4–7] Process parameters that are commonly studied are

dissolved oxygen (DO), temperature, and pH, as all have profound effects on growth, productivity, and glycosylation.[8]

Typically, the culture pH is held to a constant value or within a small range throughout the culture via pre-determined set points using either CO_2 or acid to lower the pH and base to raise the pH.[9] Alternatively, single pH shifts have been used to improve product quality, specifically charge variants.[10,11] A pH shift has been shown to impact glycosylation, where both charge variants and sialylation are critical quality attributes (CQAs).[12] Further, pH-dependent dynamic models have been developed to tune and time multiple pH shifts for a culture to increase viable cell density (VCD) and productivity.[13] Studies have also shown high-density mammalian cell cultures can be conducted without external pH control in large-scale reactors, where non-homogeneous mixing can make pH control more challenging.[14] In CO_2 controlled cultures, controlling pH to a set point can result in a heavy CO_2 burden on the cells, resulting in decreased culture performance in CHO cells as well as other cell types, including hybridoma cells.[15–17] Thus, there is a need for a tailored pH control platform that decreases CO_2 flow into the bioreactor while maintaining the repeatability of a set point pH.

In this study, a dynamic pH profile was used to determine if bioreactor productivity could be improved by using a pH profile that mimics that of an uncontrolled shake flask. The goal was to simulate the pH environment of shake flasks while still having upper and lower bounded pH control, as well as DO control. During preliminary shake flask experiments, it had been observed that the satellite shake flask cultures had better growth and productivity than the ambr250 bioreactors. One hypothesis was the pH profile differences. Therefore, the pH was monitored throughout satellite shake flask cultures to observe the natural pH drift. The dynamic pH profile was developed to mimic the natural, uncontrolled pH profile when transferred to small (250 mL) bioreactors to help address this hypothesis. Cultures were conducted with pH set-points of 6.9 ± 0.03 or 6.9 ± 0.10 and compared to cultures with the dynamic pH profile. Cultures with pH set-points of 6.9 ± 0.10 were then compared to the dynamic pH profile cultures using a glutamine-driven feeding strategy and under lactate stress. The effects of the dynamic pH profile on growth, productivity, glycosylation, and charge variants across the glutamine-driven feeding strategy and lactate stresses will be presented.

2 | MATERIALS AND METHODS

2.1 | Cell culture

Recombinant CHO-K1 Clone A11 expressing the anti-HIV antibody VRC01 (IgG_1) was obtained from the Vaccine Research Center at the National Institutes of Health (NIH). The working cell bank (WCB) has a population doubling level (PDL) of approximately 10. As per NIH instructions for this cell line, shake flask cultures are conducted at 37°C and bioreactor studies at 36.5°C.

2.1.1 | Pre-cultures

A WCB vial (1 mL frozen in liquid nitrogen) was thawed into a 125 mL baffled, vented shake flask with 30 mL working volume containing Acti-Pro media (Cytiva) with 6 mM L-glutamine (Sigma–Aldrich). Cells were maintained in a 5% CO_2 incubator at 37°C with 135 rpm orbital shaking with a 0.75-inch throw diameter. The cells were passaged and expanded every 2–3 days for at least three passages prior to inoculation into either 500 mL baffled shake flasks or the ambr250 high-throughput (HT) bioreactors. For the glutamine-driven feeding studies, cells were passaged three times in media without glutamine prior to the bioreactor experiments, and this prevents a lag phase in the bioreactor.

2.1.2 | Feeding regimens

The standard operating condition feeding strategy is a pyramid feeding regimen: Days 3–5, 3%/0.3% v/v Cell Boost 7a/7b (Cytiva); Days 6–7, 4%/0.4% v/v; Days 8–9, 5%/0.5% v/v; Days 10–11, 4%/0.4% v/v; Days 12–14, 3%/0.3% v/v, where %v/v is calculated based on current working volume for the bioreactor or shake flask. For the glutamate-driven feeding protocol, an additional 3%/0.3% v/v feed Cell Boost 7a/7b was added on Day 0. When the glutamate concentration was less than 2.5 mM, 3%/0.3% v/v Cell Boost 7a/7b was added, rather than daily additions. For the lactate-stressed cultures, 150 g/L sodium lactate was added at 12, 24, and 36-h to increase lactate by 10 mM for a total of 30 mM lactate.

2.1.3 | Bioreactor studies

The ambr250 HT bioreactors (Sartorius Stedim, Göttingen, Germany) were equipped with two pitched blade impellers and an open pipe sparger (vessel part number: 001-5G25). Bioreactors were inoculated to a target VCD of 0.4×10^6 cells/mL into 210 mL media. All cultures were supplemented with glucose daily as needed to maintain concentrations above 6 g/L. Temperature was controlled to 36.5°C. DO was controlled to 50% air saturation using a 6-level proportional-integral-derivative (PID) control algorithm.[18] The control settings for DO are listed in Table 1. For the control and lactate-stressed cultures, samples were taken daily for offline VCD, viability, glucose, glutamate, glutamine, lactate, ammonia, dissolved oxygen (pO_2), dissolved CO_2 (pCO_2), and pH beginning on day 0 and for IgG concentration beginning on day 5. For the glutamate-driven feeding scheme, sampling was the same except for glutamate, which was measured twice daily.

2.2 | pH control strategies

Three pH control strategies were employed to provide three different pH profiles (pH set-point ± deadband): pH 6.9 ± 0.03, pH 6.9 ± 0.10, or a dynamic pH profile. The dynamic pH profile was pH 7.3 ± 0.10 initially; then, on day 3, it was switched to 6.9 ± 0.10. On day 4, the

TABLE 1 PID settings for DO control in the ambr250 HT bioreactor system.

Level	Variable	Minimum	Maximum	K_p	t_I (s)	t_D (s)
0	Stir speed (rpm)	300	300	NA	NA	NA
	Gas flow rate (mL/min)	2	2			
	O_2 mix (%)[a]	0	0			
	CO_2 flow rate (mL/min)	0.1	0.1			
1	Total gas flow rate (mL/min)	2	20	0.10	0	100
2	O_2 mix (%)	0	50	0.15	0	100
3	Stir speed (rpm)	300	400	2.0	0	100
4	O_2 mix (%)	50	100	0.15	0	250
5	Stir speed (rpm)	400	800	1.0	0	100
6	O_2 flow (mL/min)	0	20	0.50	0	100

Note: Level 0 represents the initial conditions for the control manipulated variables. Level 1 increases the total gas flow rate when the DO falls below the DO set-point. No overlay gas was used. Air, O_2, and CO_2 are all provided through the sparge gas stream. NA – Not Applicable.
[a]O_2 mix is the percentage of oxygen mixed with the sparge gas, which contains air and a variable amount of carbon dioxide that is used for pH control.

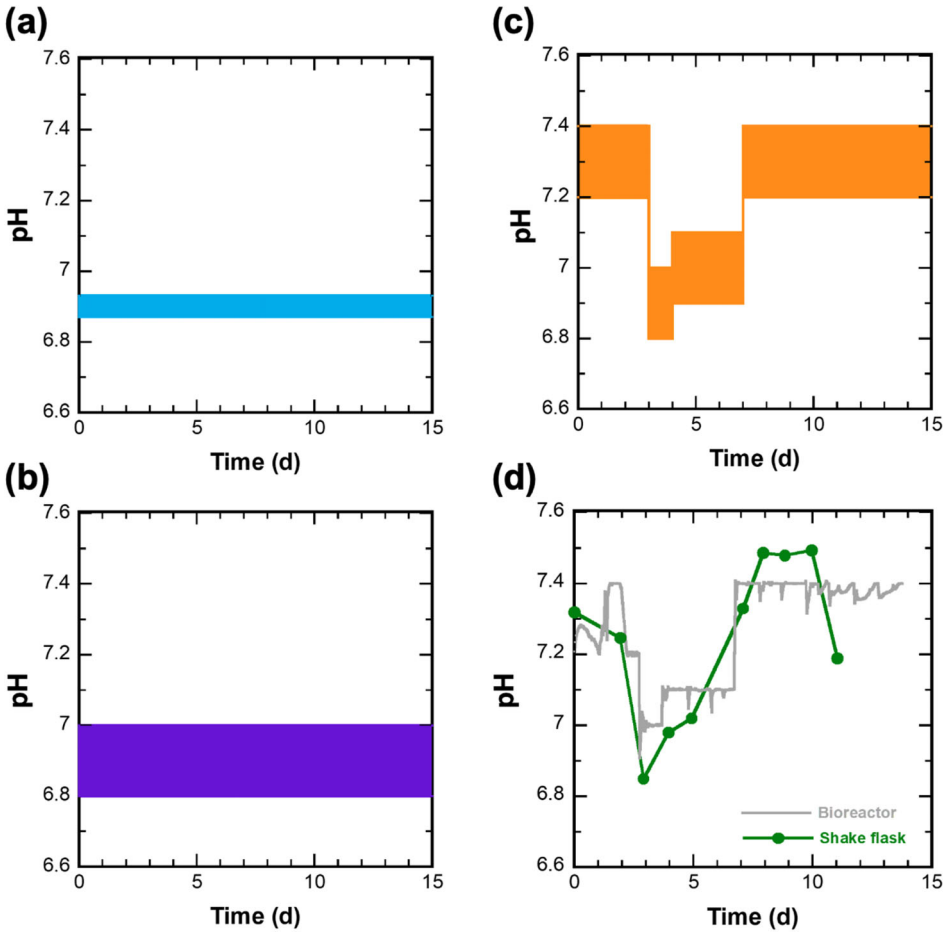

FIGURE 1 Comparison of pH profile set-points. The setpoint pH profiles (pH set-point ± deadband) for (a) 6.9 ± 0.03, (b) 6.9 ± 0.10, and (c) dynamic pH profiles. (d) Offline pH for shake flasks (green) and online pH for representative bioreactor with dynamic pH control strategy (gray).

pH profile was switched to 7.0 ± 0.10. On day 8, the pH profile was switched to 7.3 ± 0.10. Figure 1 shows these pH profiles (pH set-point ± deadband) graphically. Also shown in Figure 1 is a representative pH profile for a shake flask and a representative dynamic pH profile bioreactor. For all cultures, pH was controlled by CO_2 for the upper limit and sodium bicarbonate for the lower limit

Level	Variable	Minimum	Maximum	K_P	t_I (s)	t_D (s)
Lower	Base flow rate (mL/h)	0	1	10	0.02	100
Upper	CO_2 flow rate (mL/min)	0.1	10	10	0.00	100

TABLE 2 PID settings for pH control in the ambr250 HT bioreactor system.

with a PID control algorithm. Table 2 lists the control settings for the pH algorithm.

2.3 | Analytical methods

2.3.1 | Offline measurements

VCD and viability were measured using a Vi-Cell XR cell viability analyzer (Beckman Coulter, Brea, CA). Extracellular glucose, glutamine, glutamate, ammonia, lactate, and IgG concentrations were measured using a Cedex Bio Analyzer (Roche Diagnostics, Mannheim, Germany). Offline pH, pO_2, and pCO_2 were measured using an ABL90 FLEX PLUS blood gas analyzer (Radiometer America, Brea, CA). Samples for amino acid analysis were centrifuged at 10,000 × *g* for 10 minutes at 4°C. The supernatant was aliquoted and frozen at −20°C until analysis occurred. Amino acid concentrations were measured using the REBEL cell culture media analyzer (908 Devices, Boston, MA). End of culture harvest samples were taken for glycosylation analysis, which was conducted as described in Synoground et al.[19] In brief, a Protein A agarose resin was used to obtain the IgG_1 from the culture broth. Glycan profiles were obtained via ultra-performance liquid chromatography (UPLC). The Empower 3 software (Waters Corporation, Milford, MA) was used to analyze the chromatograms. Normalized glycan fractions were obtained.

2.3.2 | Cell specific productivity and consumption rates calculations

Integral viable cell density (IVCD) was obtained from VCD versus time area under the curve using the trapezium rule. Cell specific productivity (q_p) was calculated daily from the titer and IVCD given by the following equation:

$$q_p = \frac{Titer}{IVCD}$$

Specific amino acid consumption rates were calculated using a linear model adapted from Meadows et al. and further described in Synoground et al.[19,20]

2.3.3 | Charge variant analysis

Charge variant analysis was conducted using the ZipChip high-resolution chip for native protein analysis (HRN) (part number: 810-00227, 908 Devices Inc.) and the ZipChip Charge Variant Analysis (CVA) Kit (part number: 850-00052, 908 Devices Inc.). Harvested media was buffer exchanged to the charge variant analysis sample diluent using 7 K Zeba Spin filters (89882, Thermo Fisher Scientific). Filters were prepared according to manufacturers' instructions, washing the bed three times with the CVA diluent. Buffer-exchanged samples were loaded directly into autosampler vials. The ZipChip system and HRN chip were primed with the CVA kit background electrolyte (BGE). Samples were run with a field strength of 500 V/cm, injection volume of 1 nL, and an analysis time of 15 min. Samples were analyzed in triplicate, with a BGE refresh performed before each run. Mass spectrometer data was collected with the Exploris 240 Biopharma orbitrap mass spectrometer (Thermo Fisher Scientific). Table 3 displays the method settings and the global parameters for the data collection. Data was visualized and chromatographic peak areas were calculated using Qual Browser (Thermo Fisher Scientific), and mass spectrometry (MS) spectra were processed using BioPharma Finder 5.0 (Thermo Fisher Scientific).

TABLE 3 Exploris 240 Biopharma Orbitrap Mass Spectrometer settings and global parameters.

Parameter	Value
Application Mode	Intact Protein
Method Duration	15 min
Ion Sources Type	ESI
Gas Mode	Static
Sheath Gas (Arb)	2
Ion Transfer Tube Temp (°C)	300
Pressure Mode	Standard Pressure
Advanced Peak Determination	False
Orbitrap Resolution	30 k
Scan Range (m/z)	2000–8000
RF Lens (%)	150
AGC Target	Standard
Max. Inj. Time Mode	Custom
Max. Inj. Time (ms)	10
Microscans	3
Data Type	Profile
Polarity	Positive
Source Fragmentation	Enabled
Energy (V)	135

2.3.4 | Glycosylation analysis

Samples for glycosylation analysis were processed as described in Synoground et al.[19] Briefly, samples were collected and centrifuged at 10,000 × *g* for 15 min at 4°C. Protein A agarose resin (1 mL, Pierce,

ThermoFisher Scientific, Waltham, MA) was used to capture up to 1 mg IgG. The IgG was eluted using 10 mL elution buffer (100 mM glycine, pH = 2.75, filter sterilized), collected in 1 mL fractions. Protein-containing fractions were combined and concentrated to 100 µL via Amicon ultra-centrifugal filters (Millipore Sigma, Burlington, MA), buffer exchanged, and re-concentrated to a final volume of 20–100 µL. The purified IgG was stored at −20°C until analyzed. Glycan profiles were determined via ultra-performance liquid chromatography (UPLC). Glycans were released from the purified IgG and fluorescently labeled using the Glycoworks Rapifluor-MS N-glycan kit (Waters Corporation, Milford, MA) according to the manufacturer's protocol. Glycan identities were determined by using dextran standards (Rapifluor-MS Dextran calibration ladder, Waters Corporation, Milford, MA) to create a standard curve and comparing retention times of glycans against reference values in the "Glycostore" database (https://glycostore.org/). Empower 3 software (Waters Corporation, Milford, MA) was used for all analyses of chromatograms, and glycosylation data were analyzed as normalized peak area.

2.4 | Statistical analysis

Statistical analysis was performed using the JMP Pro 16 software (SAS Institute, Inc., Cary, NC) for replicate data. Data was first analyzed using a Generalized Linear Model ($p \leq 0.05$) to determine if the pH control strategy was an effector. For cases where the effectors were statistically significant, a Standard Least Square procedure ($p \leq 0.05$) with post-hoc Tukey analysis was conducted. Error bars on graphs represent standard deviations.

3 | RESULTS AND DISCUSSION

3.1 | Development of the dynamic pH profile

To compare the effects of a set-point pH to a pH profile that mimics uncontrolled shake flask pH profiles, a preliminary shake flask study was conducted to establish the ranges for the dynamic pH profile. Figure 1 shows a comparison of the offline pH for a typical shake flask culture and the online pH for a representative dynamic pH profile ambr250 HT bioreactor. These profiles indicate that the uncontrolled pH in the shake flask and the dynamic pH profile in the bioreactors were well matched.

3.2 | Effects of pH control strategy on culture outcomes

3.2.1 | Cell growth and productivity

To investigate the impact of pH on CHO VRC01, three pH profiles were used for cultures with the standard feeding protocol. The three pH profiles were (pH set-point ± deadband): 6.9 ± 0.03, 6.9 ± 0.10, or a dynamic pH profile. The growth, titer, and cell specific productivity (q_p), glucose, lactate, and ammonia profiles are shown in Figure 2. All cultures had similar growth trends and maximum VCD regardless of the pH profile used. Cell viabilities were similar, and these profiles are shown in the Supporting Information, as well as the pH profiles. In comparison, the titers were significantly different, where the dynamic pH profile cultures had the highest final titer. The dynamic pH profile also had the highest cell specific productivity overall compared to the pH 6.9 ± 0.03 and pH 6.9 ± 0.10 cultures. The initial high standard deviation observed for the pH 6.9 ± 0.03 cultures was due to the low titers and high coefficient of variation (CV) (titers 0.2, 0.21, and 0.34 g/L and 31% CV). The culture with the 0.10 pH deadband had a higher titer than the 0.03 pH deadband. Yet, the cell specific productivities were similar over most of the culture time.

The dynamic pH profile had higher lactate levels than the pH 6.9 ± 0.03 and pH 6.9 ± 0.10 cultures. In contrast, the dynamic pH profile had lower ammonia accumulation compared to the pH 6.9 ± 0.03 and pH 6.9 ± 0.10 cultures. Both lactate and ammonia are historically considered to be inhibitory byproducts of metabolism, and their reduction in cell culture is of interest for both industrial and academic research.[21] Although there is higher lactate accumulation during the exponential growth phase in the cultures with lower CO_2, all three cultures still exhibit the critical shift between lactate production and consumption that is characteristic of a culture that achieves longer culture times and higher final titers.[22] Additionally, none of the cultures exhibit lactate accumulation above the inhibitory threshold of 5.4 g/L.[23,24] Alternatively, the dynamic pH profile significantly reduces the amount of ammonia (NH_3) present after culture day 7. This is beneficial as ammonia accumulation has been linked to decreased growth and antibody titers above a threshold of 5 mM.[21,23] Previous work has shown that elevated pCO_2 in fed-batch cultures contributes to increased ammonia accumulation, and this work further supports this claim.[22]

Figure 2 also shows the CO_2 inlet flow rate, off-gas CO_2 levels, and the offline dissolved carbon dioxide (pCO_2) for the three pH control strategy cultures. The dynamic pH profile cultures had the lowest CO_2 flow rates, lowest off-gas CO_2 levels, and lowest pCO_2 levels. It is common that CO_2 build-up in fed-batch cultures results in growth inhibition and lower cell specific productivity.[15,16] The findings of this study are consistent with previous observations and further demonstrate that lower pCO_2 leads to better culture performance. When CO_2 is used to control the pH to a setpoint and CO_2 removal is not sufficient, the pCO_2 levels will increase dramatically. As CO_2 is non-polar, it can readily diffuse across the cell membrane where dissociation into H^+ and HCO_3^- occurs through hydration.[25] Therefore, high pCO_2 levels are likely to change the intracellular pH of the cell, even if the external media pH is controlled to a set-point.[26] The change in intracellular pH must be counteracted by the Na^+/H^+ exchanger.[27] In order for the cell to utilize this transporter to maintain a stable intracellular pH, adenosine triphosphate (ATP) must be shuttled toward maintaining the sodium gradient necessary for the antiporter to operate. With more ATP needed to drive the exchanger, less ATP is available for cell growth and protein synthesis. According to a study conducted by Thorens and Vassali, high pCO_2 levels also have the

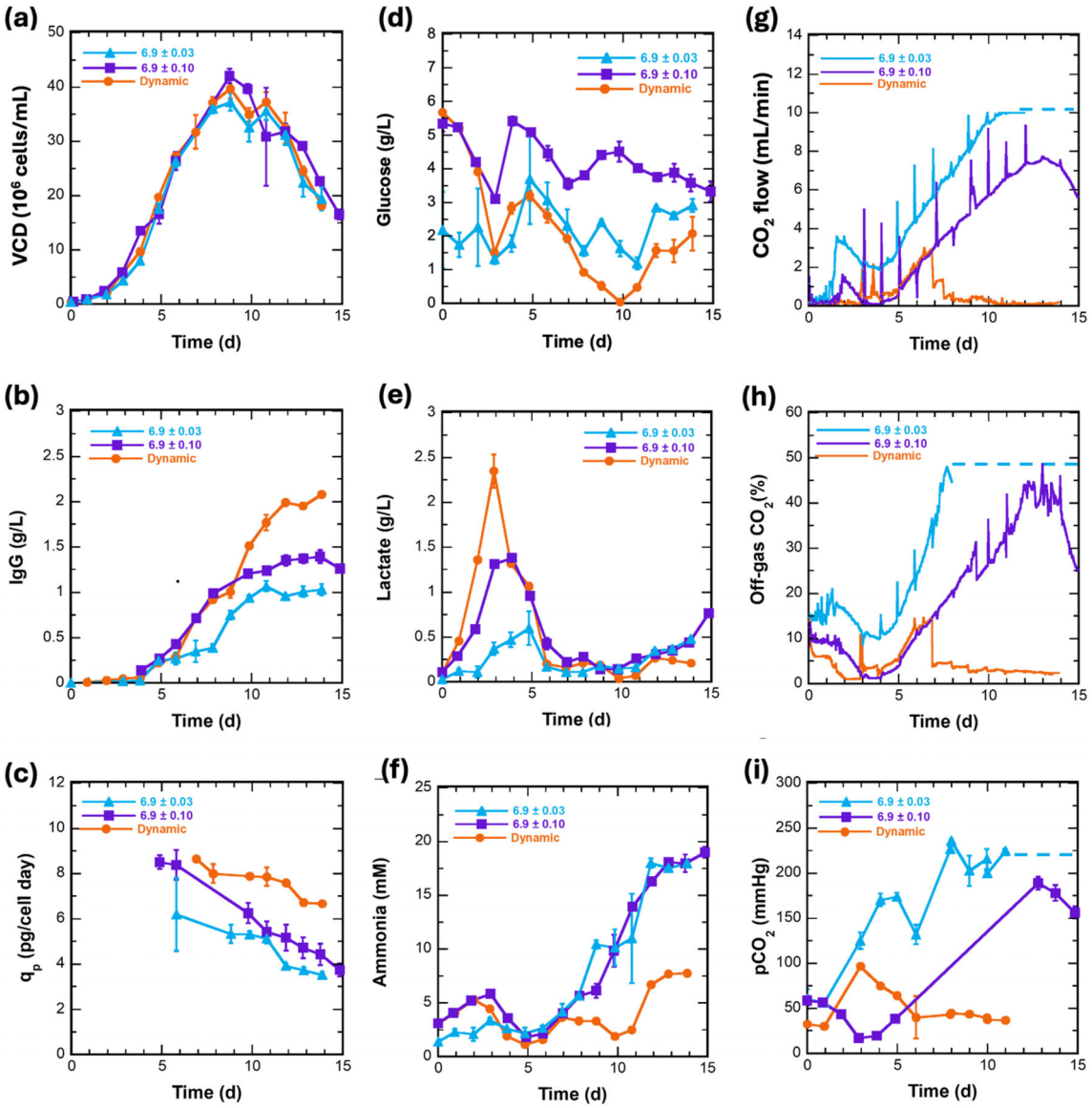

FIGURE 2 Growth, productivity, and gassing characteristics for standard operating condition cultures with varying pH control strategies. (a) VCD, (b) titer, (c) cell specific productivity (q_p), (d) glucose, (e) lactate, (f) ammonia, (g) CO_2 flow rate (h) off-gas CO_2 levels, and (i) dissolved CO_2 (pCO_2) levels. pH 6.9 ± 0.03 (light blue triangles), pH 6.9 ± 0.10 (purple squares), and dynamic pH profile (orange circles). The CO_2 flow sensor and the off-gas CO_2 sensor cannot read above 10 mL/min and 50%, respectively, indicated by the dashed line. Values above these thresholds are shown as dashed lines. Error bars represent standard deviation ($N = 3$).

potential to change the pH in the endoplasmic reticulum and Golgi, where key protein processing occurs.[28] This, combined with the shortage of ATP available, results in lower overall culture productivity. It has been previously reported that pCO_2 levels above 150 mmHg are inhibitory to cell growth and productivity.[29] This study shows similar findings, where only the dynamic pH profile maintains pCO_2 values below this threshold.

3.2.2 | Amino acid consumption rates

To confirm the positive effects of decreased pCO_2 on CHO cell metabolism, amino acid concentrations for pH 6.9 ± 0.10 and the dynamic pH profiles were evaluated, as these cultures had the highest productivity. Cell-specific amino acid consumption rates were calculated over the exponential growth phase of the culture. Figure 3 shows the cell-specific amino acid consumption rates for the standard operating condition cultures at pH 6.9 ± 0.10 and the dynamic pH profile that had statistically different consumption rates between the conditions. All amino acid concentration profiles are shown in the Supporting Information. The dynamic pH profile has higher consumption rates across the measured amino acids ($p \leq 0.05$). This confirms the positive correlation between pH, decreased pCO_2, and improved metabolism because of increased ATP availability.

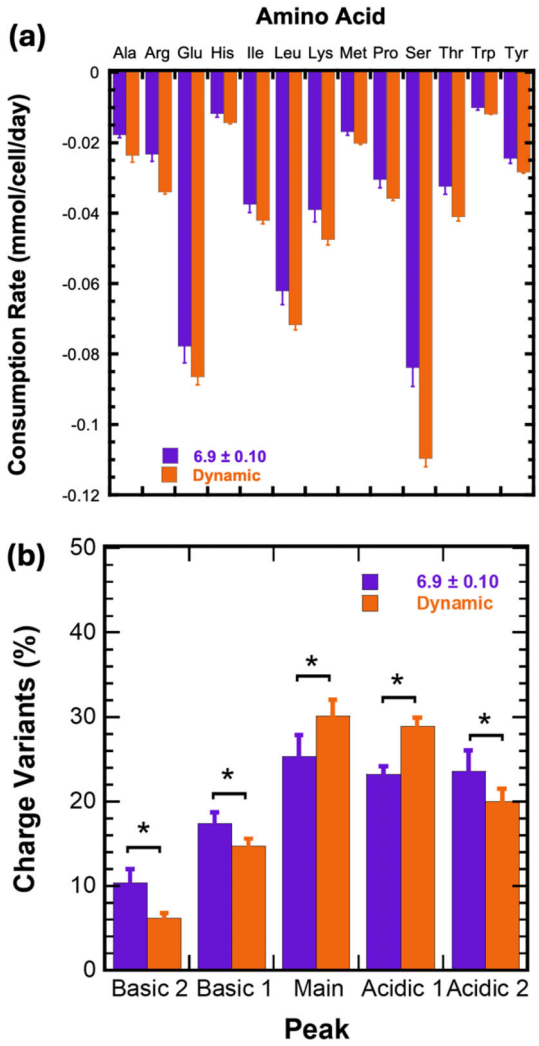

FIGURE 3 Effect of pH control strategy for standard operating condition cultures on cell specific amino acid consumption rates and charge variant profiles. (a) Cell specific amino acid consumption rates for amino acids with statistically significant net consumption differences. (b) Charge variants. pH 6.9 ± 0.10 (purple), dynamic pH profile (orange). Asterisks represent statistically significant differences ($p \leq 0.05$). Error bars represent standard deviation ($N = 3$).

3.2.3 | Charge variant analysis

To further evaluate pH profile impacts on product quality, charge variant analysis was conducted for the pH 6.9 ± 0.10 and dynamic pH profile cultures. Charge variants were analyzed using the ZipChip charge variant analysis kit from 908 Devices Inc. Peaks were classified as either basic 1, basic 2, main, acidic 1, or acidic 2 and were found to differ mainly by the degree of sialylation of the glycans. It is important to note that the structure of the VRC01 mAb has a second glycosylation site. This directly impacts the information gained from CVA-MS due to increased complexity. Figure 3 shows the percentage of charge variant species for the pH 6.9 ± 0.10 and dynamic pH cultures. The dynamic pH profile cultures had the highest fraction of main and acidic 1 peaks and the lowest fraction of basic 1, basic 2, and acidic 2 peaks. An increase in the main peak percentage is important as both acidic and basic variants have the potential to impact the structure and biological activity of the protein.[30] In general, acidic variants are more detrimental to antibody activity than basic variants.[31] The mechanism by which a basic variant is formed is critical in determining its impact. For example, if a basic species arises due to isomerization or succinimide, there may be inactivation of the molecule or an illicit immune response.[32] However, if a basic variant is a result of a C-terminal lysine/arginine, C-terminal amination, or N-terminal pyro glutamate, there should be no impact on the efficacy or potency of the antibody.[33–35] While charge variants caused by sialic acid residues are easily observed, due to the complexity of the VRC01 mAb's glycosylation profile, further analysis, such as peptide mapping, is needed to determine whether any detrimental post translational modifications described above are present on the molecule.

3.2.4 | Glycosylation analysis

To evaluate the impact of pH on product quality, the effects of the dynamic pH profile on glycosylation for the control and pH 6.9 ± 0.10 cultures were assessed since they had the highest productivity. Figure 4 shows the glycosylation profiles for these two cultures. Cultures with the dynamic pH profile had an increase in G0F-N, G0, G1, G1FS1, and G2FS1 glycoforms, with increases in G0F-N, G0, G0F, and G1FS1 having statistical significance ($p \leq 0.05$). This increase was accompanied by a decrease in the G1F and G2F glycoforms for the dynamic pH profile cultures. The dynamic pH profile had an increase in G0 terminal galactosylation forms, but a decrease in G1 and G2 galactosylation forms. This is not necessarily beneficial as higher levels of terminal galactosylation have been correlated with higher antibody-dependent cellular cytotoxicity (ADCC) activity, which contributes to antibody binding and clinical efficacy.[36,37] There is a statistically significant increase in sialylation when the dynamic pH profile is implemented compared to the set-point pH 6.9 ± 0.10. This is beneficial as more sialylated glycoforms have been shown to have a longer in vivo half-life.[38,39] There is no statistical difference in fucosylation when implementing the dynamic pH profile. This is ideal as increases in fucosylation have been correlated with decreased ADCC activity and decreased FcγRIIIa and FcγRIIb binding affinity.[40–43]

3.3 | Effectiveness of dynamic pH control strategy for stressed cultures

3.3.1 | Cell growth and productivity for stressed cultures

To characterize the effects of the pH 6.9 ± 0.10 and dynamic pH profile across culture conditions, these two pH control strategies were used for glutamate-driven feeding and lactate-stressed cultures. These other culture conditions were examined to ensure that the observations are not specific to the standard operating conditions and

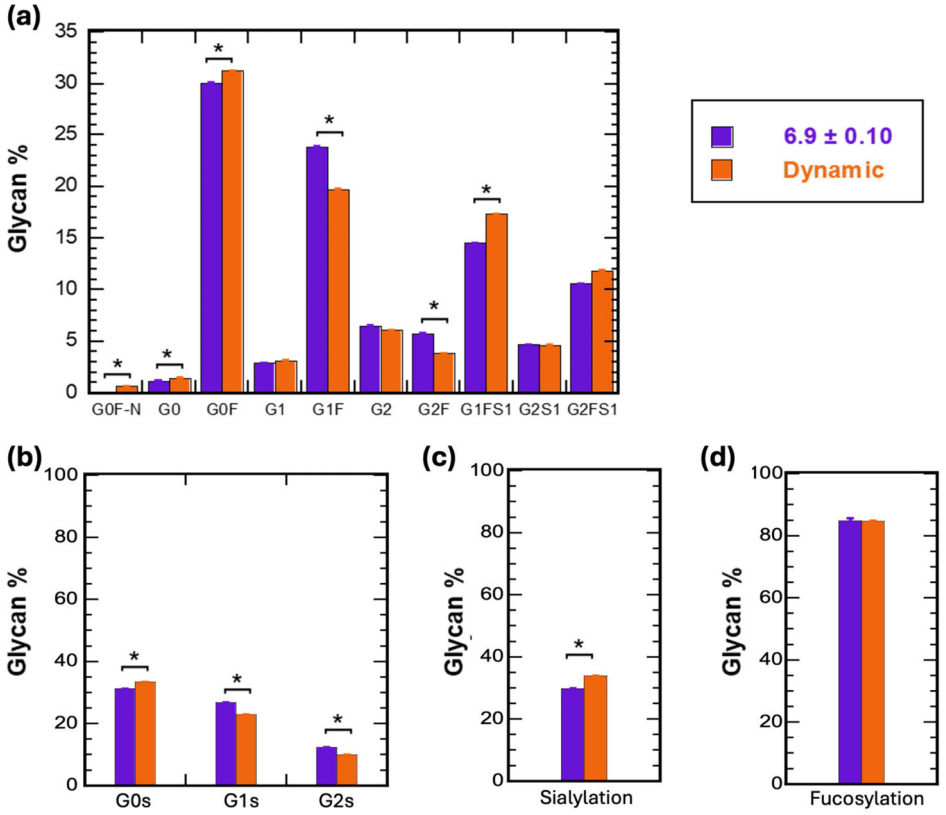

FIGURE 4 Effect of pH control strategy on glycosylation profiles. (a) total glycosylation, (b) terminal galactosylation, (c) sialylation, and (d) fucosylation. pH 6.9 ± 0.10 (purple), dynamic pH profile cultures (orange) ($N = 3$). Asterisks represent differences that are statistically significant ($p \leq 0.05$). Error bars represent standard deviation.

hold true under different metabolic states. These two pH control strategies were selected because standard operating condition cultures with these pH control strategies had the highest productivity. The glutamate-driven feeding was selected to evaluate the impacts of a dynamic pH profile with varying nutrient availability. The glutamate-driven feed culture exhibited less overall feed volume added to the culture and, therefore, less nutrient availability. Glutamate was selected as the amino acid of choice due to analytical availability within minutes of sampling via the Cedex Bioanalyzer. Similarly, the lactate-stressed culture was chosen to act as a representative culture for cell stress. Both of these stressful culture conditions were evaluated to ensure consistency of findings across culture conditions. Figure 5 shows the growth and productivity profiles for the glutamate-driven and lactate-stressed cultures with pH 6.9 ± 0.10 as well as the dynamic pH profile. The maximum VCD was higher in both the glutamate-driven feeding and lactate-stressed cultures with the dynamic pH profile. For the standard cultures, the dynamic pH profile had no effect on the maximum VCD, suggesting there is a separate limiting factor capping the culture at 40×10^6 cells/mL. The large standard deviation in titers at the end of the lactate dynamic cultures is the result of one of the dynamic pH cultures having a significantly lower titer than the other, where the higher titer lactate culture reached a titer over 2 g/L, which was similar to the titers observed for the paired standard operating condition cultures without stress. So, despite the higher standard deviation observed for the lactate-stressed cultures, the dynamic pH profile cultures had higher titers and cell specific productivity for both the glutamate-driven feeding and lactate-stressed conditions.

To confirm the consistency of the dynamic pH profile impact on inhibitory byproducts, lactate and ammonia concentrations for the glutamate-driven and lactate-stressed cultures were evaluated. Figure 5 shows the lactate and ammonia profiles for the glutamate-driven feeding and lactate-stressed conditions for the pH 6.9 ± 0.10 and the dynamic pH profile cultures. Overall, the dynamic pH cultures had higher lactate levels during the exponential growth phase. However, cultures with the dynamic pH profile also had lower levels of ammonia accumulation. The lactate-stressed cultures with pH 6.9 ± 0.10 had higher lactate accumulation compared to all other conditions beginning on day 9. Exponential accumulation of lactate near the end of the lactate-stressed cultures could be attributed to extrachromosomal overexpression of *Akr1b1*, a gene closely linked to Warburg metabolism in some cancer types.[44]

Figure 6 highlights the CO_2 flow rates and off-gas CO_2 levels for the glutamate-driven and lactate-stressed cultures with pH 6.9 ± 0.10 and the dynamic pH profile. For both culture conditions, the dynamic pH profile had lower CO_2 flow rates as well as lower off-gas CO_2 levels. The improved productivity in the glutamate-driven feeding and lactate-stressed culture conditions can be attributed to decreased pCO_2. For the glutamate-driven feeding, there was a 73% increase in titer and a 54% increase in cell-specific productivity at the time of harvest. Lactate-stressed cultures with the dynamic pH profiles had a 200% increase in titer and a 150% increase in cell-specific

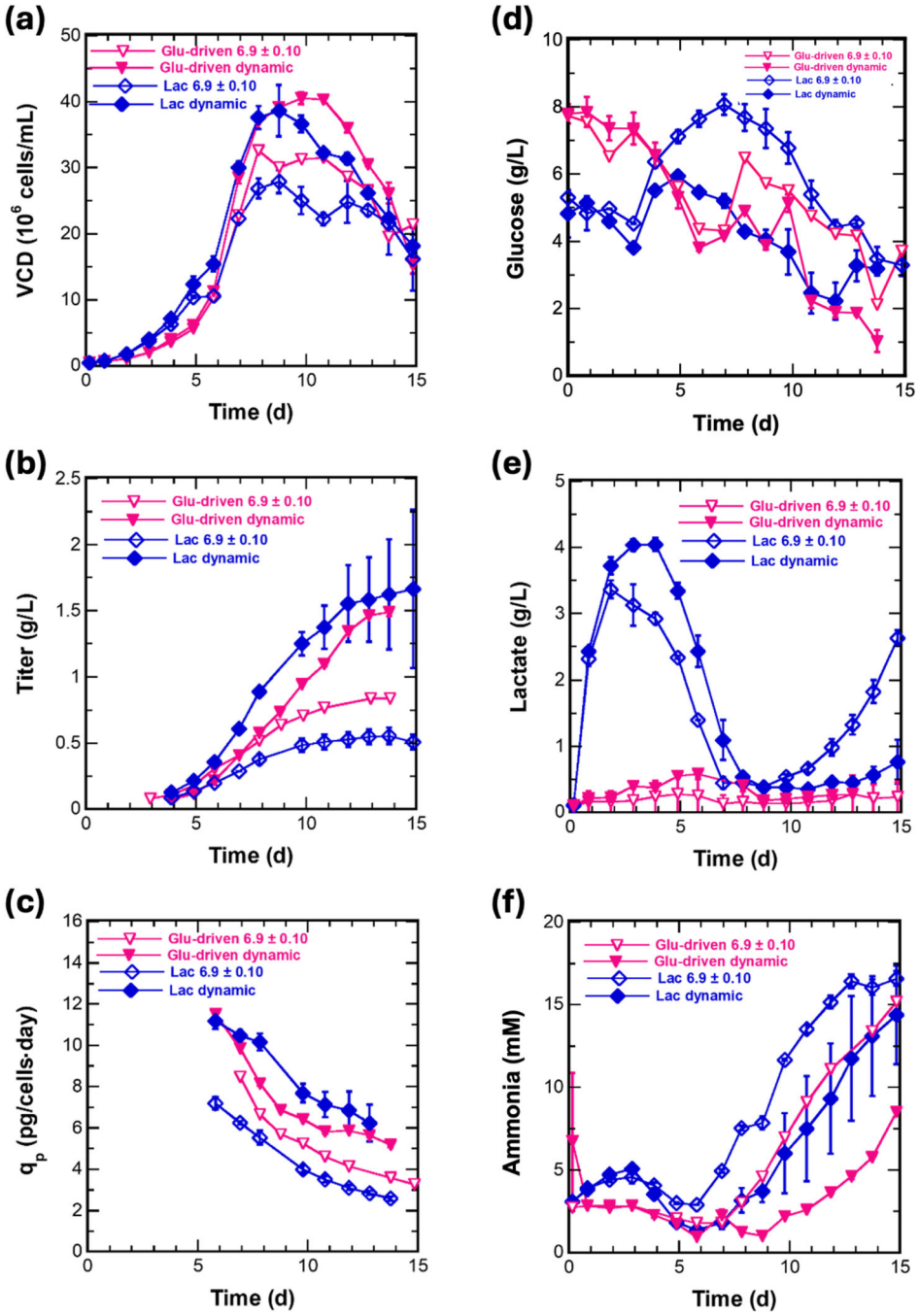

FIGURE 5 Effect of pH control strategy on growth and productivity characteristics for glutamate-driven feeding and lactate stressed cultures. (a) VCD, (b) titer, and (c) cell specific productivity (q_p), (d) glucose, (e) lactate, and (f) ammonia. Glutamate-driven feeding cultures are (pink downwards triangles), lactate stressed cultures (blue diamonds). pH 6.9 ± 0.1 (hollow symbols), dynamic pH (solid symbols) ($N = 2$). Error bars represent standard deviation.

productivity at the time of harvest compared to the standard single pH set-point control strategy cultures.

Since the glutamate-driven and lactate-stressed cultures had different VCD profiles depending on the pH control, specific production and consumption rates of lactate and ammonia were calculated. To examine production and consumption rates for lactate, the culture was divided into two phases: the initial lactate production phase and the subsequent lactate consumption phase. For the glutamate-driven feeding and lactate-stressed cultures, there was no statistical difference between the rates of lactate production or consumption ($p \leq 0.05$).

To evaluate consumption and production rates for ammonia, the culture was divided into three phases: the initial ammonia production phase, the subsequent ammonia consumption phase, and the final ammonia production phase. There was no statistical difference between the initial specific ammonia production rates and subsequent

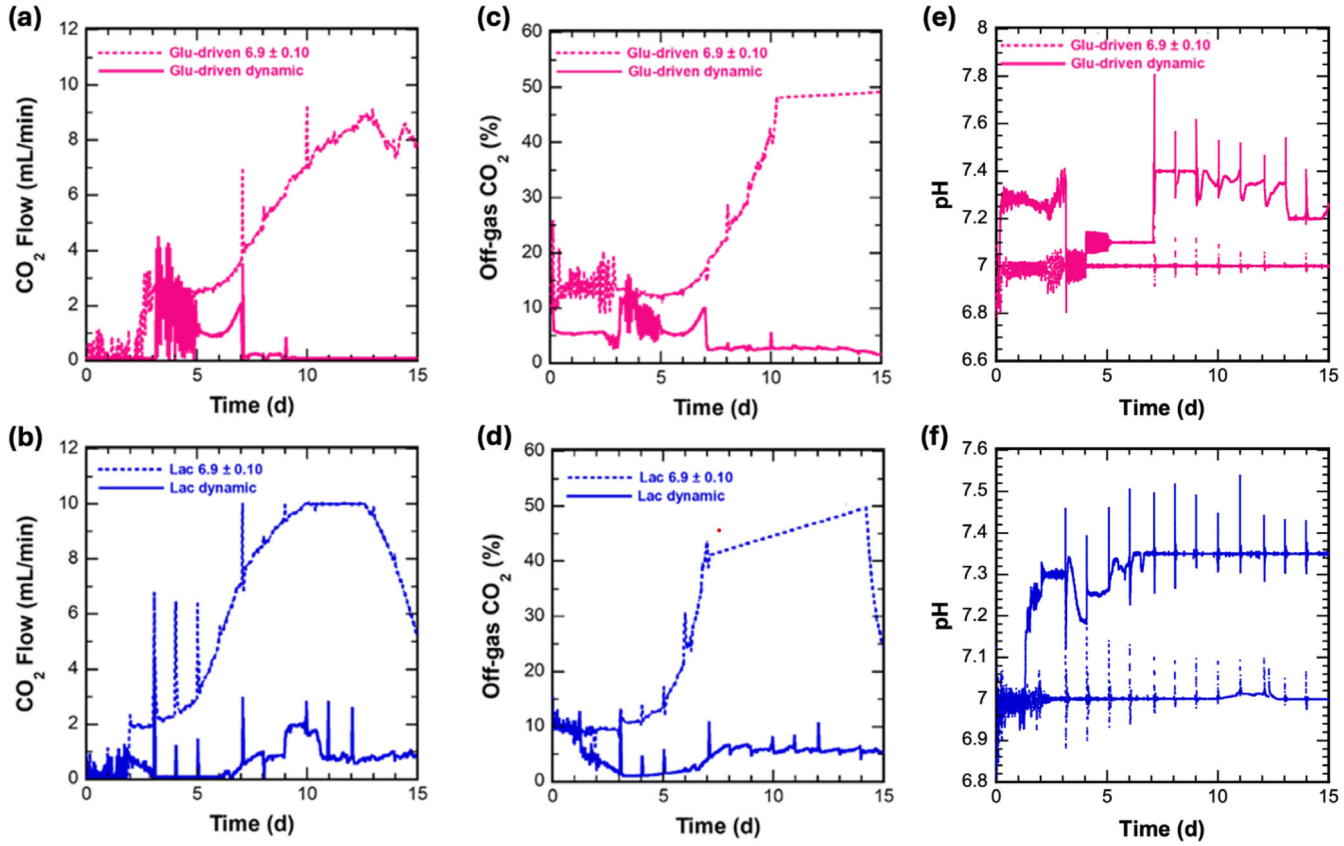

FIGURE 6 Effect of pH control strategy on CO_2 flow rates and off-gas CO_2 levels for representative glutamate-driven feeding and lactate stressed cultures. (a) CO_2 flow glutamate-driven feeding and (b) CO_2 flow lactate-stressed cultures. (c) off-gas CO_2 levels glutamate-driven feeding and (d) off-gas CO_2 levels lactate-stressed cultures. (d) pH glutamate-driven feeding and (f) pH lactate-stressed cultures. Glutamate-driven feeding cultures (pink). Lactate stressed cultures (blue). pH 6.9 ± 0.01 cultures (dashed lines), dynamic pH cultures (solid lines).

consumption rates in either the glutamate-driven or lactate stressed cultures. However, the final specific ammonia production rates were significantly different ($p \leq 0.05$) for the glutamate-driven cultures, with the dynamic pH culture having less overall ammonia accumulation compared to pH 6.9 ± 0.10 cultures. Conversely, the lactate stressed cultures had no difference between the cell specific ammonia production rates in the pH 6.9 ± 0.10 or the dynamic pH cultures. As the single pH set-point control and glutamate-driven feeding cultures had lower cell specific ammonia production at the end of culture, this suggests that the lower CO_2 flow and off-gas CO_2 due to the dynamic pH control had positive effects on ammonia accumulation in high cell density fed-batch cultures.

3.3.2 | Charge variant analysis of stressed cultures

To confirm consistent impacts of the pH profile on charge variants across culture conditions, analysis was conducted for the glutamate-driven feeding cultures with the set-point pH 6.9 ± 0.10 and dynamic pH profiles. Charge variant analysis for the lactate stressed cultures was not conducted as this condition is not considered industrially relevant. Figure 7 shows the percentage of charge variant species with

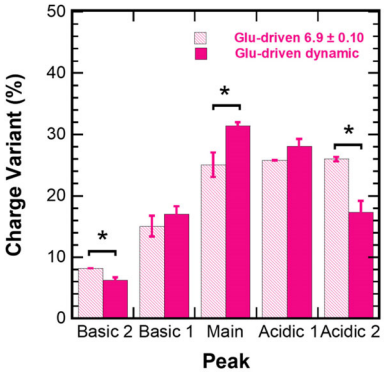

FIGURE 7 Effect of pH control strategy on charge variants for glutamate-driven feeding cultures. Cultures with pH 6.9 ± 0.10 (pink striped bars) ($N = 1$) ($n = 3$). Cultures with dynamic pH profiles (pink solid bars) ($N = 2$) ($n = 3$). N represents the number of bioreactors for a particular condition and n represents number of replicate measurements for a sample. Asterisks represent significant differences ($p \leq 0.05$). Error bars represent standard deviation.

set-point pH 6.9 ± 0.10 and the dynamic pH profile for the glutamate-driven feeding cultures. The dynamic pH profile cultures had increases basic 1, main, and acidic 1 peaks. This was accompanied by decreases

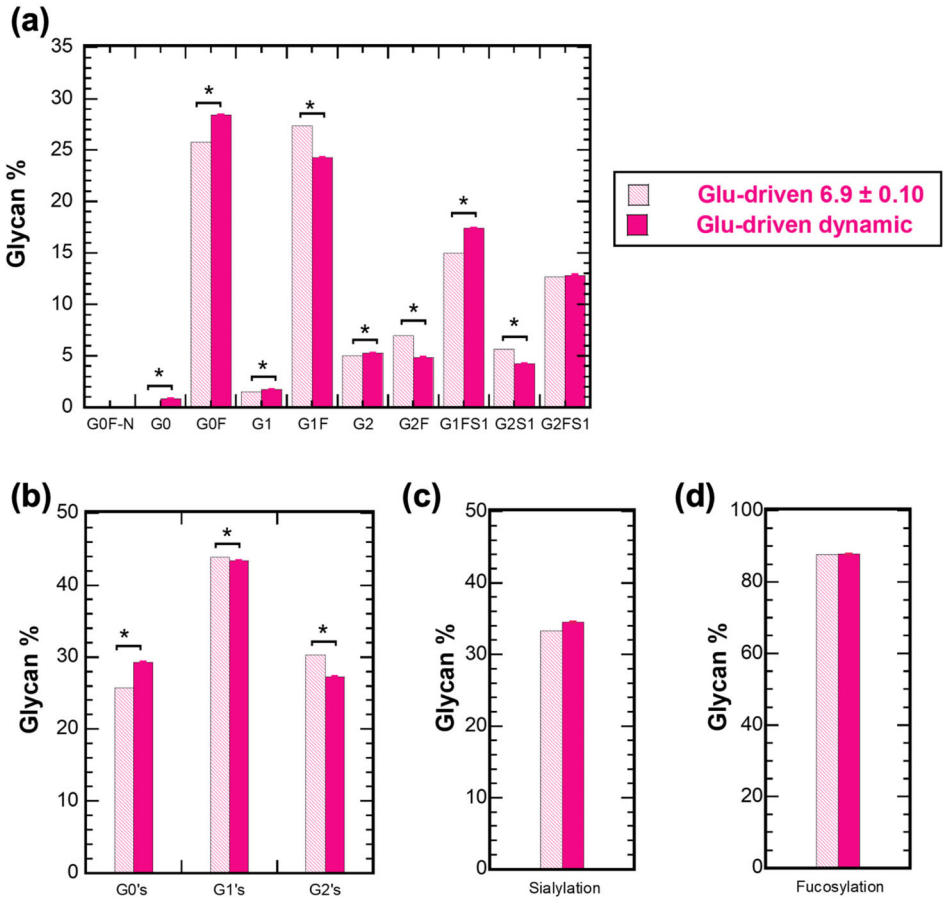

FIGURE 8 Effect of pH control strategy on glycosylation for glutamate-driven feeding cultures. (a) Total glycosylation, (b) terminal galactosylation, (c) sialylation, and (d) fucosylation. pH 6.9 ± 0.10 cultures (pink striped bars) ($N = 1$), dynamic pH profile cultures (pink solid bars) ($N = 2$). Asterisks represent significant differences ($p \leq 0.05$). Error bars represent standard deviations.

basic 2 and acidic 2 peaks. Compared to the standard operating condition cultures (Figure 3), the glutamate-driven cultures have a similar trend for basic 2, main, and acidic 2 peaks. However, unlike the standard operating condition cultures, the glutamate-driven cultures had an increase in the basic 1 peak and no change in the acidic 1 peak when cultured with the dynamic pH profile. This is considered a positive trend in the charge variant profile as, in both cases, the main peak is increasing in its contribution to the makeup of the mAb variants when the dynamic pH profile is implemented. The charge variant profile is slightly more favorable with the glutamate-driven feeding cultures compared to the standard operating condition cultures since there is less of an increase in the acidic 1 peak. These results indicate that the dynamic pH profile has a positive impact on the charge variant profile across multiple culture conditions.

3.3.3 | Glycosylation analysis of stressed cultures

To confirm consistency of the effects of the dynamic pH profile on product quality across conditions, the effects of pH profile on glycosylation were assessed for the glutamate-driven feeding strategy. Evaluation of critical quality attributes for the lactate stressed cultures was omitted, as the lactate stress condition is not industrially relevant. Figure 8 shows the glycosylation profile for the glutamate-driven feeding cultures with a pH set-point of 6.9 ± 0.10 and the dynamic pH profile. There was an increase in the G0, G0F, G1, G2, and G1FS1 glycoforms when the dynamic pH profile was used. Similarly to the standard operating condition cultures, for the glutamate-driven case, the dynamic pH profile resulted in an increase in G0 terminal galactosylation forms, but a decrease in G1 and G2 terminal galactosylation forms. Unlike the standard operating condition cultures, for the glutamate-driven cultures, there is no significant difference in the sialylation profiles. Finally, the glutamate-driven feed cultures have no change in fucosylation with the different pH profiles. Some of the presented shifts in glycosylation patterns are inconsistent with previous work that has shown that lower pCO_2 results in a shift away from G0F and G0 and toward G2F, suggesting that something other than the lower pCO_2 because of the dynamic pH profile is at work in moving these profiles.[5] Additionally, lower cell specific productivity has been shown to allow for more mature glycoforms, including G2F.[42] The cell specific productivity of the dynamic pH cultures was shown to be higher in both the standard operating condition cultures (Figure 2) and the glutamate-driven feed cultures (Figure 5). This offers an explanation as to the cause of the shift away from the more mature G1 and G2 glycoforms. This also suggests that the cell specific productivity may be a more impactful factor in determining the extent of galactosylation than pCO_2. The favorable increase of sialylation as demonstrated by the increase in G1FS1 in the dynamic pH case goes hand-in-hand with an unfavorable decrease in more mature galactosylation forms, which is an important consideration when moving

forward with implementing dynamic pH profiles in CHO cell culture as there is a clear trade-off between cell specific productivity and glycosylation profiles.

4 | CONCLUSIONS

In this study, a multi-shift dynamic pH profile was compared to traditional tight pH deadband (6.9 ± 0.03) and wide pH deadband 6.9 ± 0.10 controls in fed-batch reactors cultured using a standard operating condition with bolus feeding and no additional stressors. The results demonstrate a clear correlation between decreased CO_2 and increased volumetric and cell specific productivities because of dynamic pH control. Previous studies have assessed the possibility of conducting fed-batch cultures with varying upper pH set-points, but none of the cultures required any pH adjustment, therefore no conclusion can be made on the impact of pH profiles as a means of decreasing pCO_2 and the resulting impact on productivity.[14] The data presented in this work bridges the gap of evaluating pH strategies and CO_2 build-up in fed-batch cultures. This work was able to successfully achieve varying levels of pCO_2 in fed-batch cultures and effectively demonstrate that subsequent impacts on growth, metabolism, productivity, and product quality. The findings of this study illustrate the importance of decreased pCO_2 for cell culture productivity on a volumetric and per cell basis. The results have also demonstrated the importance of this phenomenon in a variable feeding strategy as well as a lactate stressed condition. Finally, variables impacting glycosylation in IgG molecules is a high demand area in need of elucidation. As this study was conducted for a single IgG molecular in a clonal cell line, broadening the approach to other molecules and cell lines should be explored. The findings presented demonstrate that between CO_2 levels and cell specific productivity, two previous areas of interest as drivers of glycosylation, cell specific productivity may be the stronger factor in determining the maturity of the glycoforms, which has not previously been reported.

AUTHOR CONTRIBUTIONS

Dr. Stephanie R. Klaubert performed the roles of conceptualization, investigation, writing, methodology, formal analysis, data curation, visualization, and validation. Dr. Dylan G. Chitwood performed the roles of investigation, reviewing, and editing. Dr. Danqia Peng performed the roles of investigation, reviewing, editing, formal analysis, and methodology. Dr. Erin Redman performed the roles of investigation, reviewing, editing, methodology, and formal analysis. Ji Young L. Anderon performed the roles of reviewing, editing, resources, and visualization. Dr. Nicholas R. Sandoval performed the roles of investigation, reviewing, editing, and supervision. Dr. Sarah W. Harcum performed the roles of conceptualization, investigation, funding acquisition, reviewing, editing, methodology, and supervision.

ACKNOWLEDGMENTS

The material is based upon work supported by the National Science Foundation under Grant No. OIA-1736123. Images created with BioRender.

CONFLICT OF INTEREST STATEMENT

The authors declare no conflicts of interest.

DATA AVAILABILITY STATEMENT

The data that support the findings of this study are available from the corresponding author upon reasonable request.

ORCID

Stephanie R. Klaubert https://orcid.org/0009-0005-7794-5680
Sarah W. Harcum https://orcid.org/0000-0001-9417-0489

REFERENCES

1. Klaubert SR, Chitwood DG, Dahodwala H, et al. Method to transfer Chinese hamster ovary (CHO) batch shake flask experiments to large-scale, computer-controlled fed-batch bioreactors. *Methods in Enzymology on CD-ROM/Methods in Enzymology*. Academic Press; 2021:297-320. doi:10.1016/bs.mie.2021.05.005
2. Dahodwala H, Lee KH. The fickle CHO: a review of the causes, implications, and potential alleviation of the CHO cell line instability problem. *Curr Opin Biotechnol*. 2019;60:128-137. doi:10.1016/j.copbio.2019.01.011
3. Walsh G, Walsh E. Biopharmaceutical benchmarks 2022. *Nat Biotechnol*. 2022;40(12):1722-1760. doi:10.1038/s41587-022-01582-x
4. Handlogten MW, Lee-O'Brien A, Roy G, et al. Intracellular response to process optimization and impact on productivity and product aggregates for a high-titer CHO cell process. *Biotechnol Bioeng*. 2018;115(1):126-138. doi:10.1002/bit.26460
5. Wang C, Wang J, Chen M, Fan L, Zhao L, Tan WS. Ultra-low carbon dioxide partial pressure improves the galactosylation of a monoclonal antibody produced in Chinese hamster ovary cells in a bioreactor. *Biotechnol Lett*. 2018;40(8):1201-1208. doi:10.1007/s10529-018-2586-4
6. Craven S, Shirsat N, Whelan J, Glennon B. Process model comparison and transferability across bioreactor scales and modes of operation for a mammalian cell bioprocess. *Biotechnol Prog*. 2012;29(1):186-196. doi:10.1002/btpr.1664
7. Sumit M, Dolatshahi S, Chu AHA, et al. Dissecting N-glycosylation dynamics in Chinese hamster ovary cells fed-batch cultures using time course omics analyses. *iScience*. 2019;12:102-120. doi:10.1016/j.isci.2019.01.006
8. Borys MC, Linzer DIH, Papoutsakis ET. Culture pH affects expression rates and glycosylation of recombinant mouse placental lactogen proteins by Chinese hamster ovary (CHO) cells. *Nat Biotechnol*. 1993;11(6):720-724. doi:10.1038/nbt0693-720
9. Ahleboot Z, Khorshidtalab M, Motahari P, et al. Designing a strategy for pH control to improve CHO cell productivity in bioreactor. *Avicenna J Med Biotechnol*. 2021;13(3):123-130. doi:10.18502/ajmb.v13i3.6365
10. Horvath B, Mun M, Laird MW. Characterization of a monoclonal antibody cell culture production process using a quality by design approach. *Mol Biotechnol*. 2010;45(3):203-206. doi:10.1007/s12033-010-9267-4
11. Xie P, Niu H, Chen X, et al. Elucidating the effects of pH shift on IgG1 monoclonal antibody acidic charge variant levels in Chinese hamster ovary cell cultures. *Appl Microbiol Biotechnol*. 2016;100(24):10343-10353. doi:10.1007/s00253-016-7749-4
12. Nagashima H, Watari A, Shinoda Y, Okamoto H, Takuma S. Application of a quality by design approach to the cell culture process of monoclonal antibody production, resulting in the establishment of a design space. *J Pharm Sci*. 2013;102(12):4274-4283. doi:10.1002/jps.23744
13. Hogiri T, Tamashima H, Nishizawa A, Okamoto M. Optimization of a pH-shift control strategy for producing monoclonal antibodies in Chinese hamster ovary cell cultures using a pH-dependent dynamic

model. *J Biosci Bioeng*. 2018;125(2):245-250. doi:10.1016/j.jbiosc.2017.08.015
14. Xu S, Chen H. High-density mammalian cell cultures in stirred-tank bioreactor without external pH control. *J Biotechnol*. 2016;231:149-159. doi:10.1016/j.jbiotec.2016.06.019
15. Xing Z, Kenty BM, Li ZJ, Lee SS. Scale-up analysis for a CHO cell culture process in large-scale bioreactors. *Biotechnol Bioeng*. 2009;103(4):733-746. doi:10.1002/bit.22287
16. Mostafa SS, Gu XS. Strategies for improved dCO_2 removal in large-scale fed-batch cultures. *Biotechnol Prog*. 2003;19(1):45-51. doi:10.1021/bp0256263
17. deZengotita VM, Kimura R, Miller WM. Effects of CO_2 and osmolality on hybridoma cells: growth, metabolism and monoclonal antibody production. *Cytotechnology*. 1998;28(1/3):213-227. doi:10.1023/a:1008010605287
18. Harcum SW, Elliott KS, Skelton BA, Klaubert SR, Dahodwala H, Lee KH. PID controls: the forgotten bioprocess parameters. *Discover. Chem Eng*. 2022;2(1). doi:10.1007/s43938-022-00008-z
19. Synoground BF, McGraw CE, Elliott KS, et al. Transient ammonia stress on Chinese hamster ovary (CHO) cells yield alterations to alanine metabolism and IgG glycosylation profiles. *Biotechnol J*. 2021;16(7):2100098. doi:10.1002/biot.202100098
20. Meadows AL, Kong B, Berdichevsky M, et al. Metabolic and morphological differences between rapidly proliferating cancerous and Normal breast epithelial cells. *Biotechnol Prog*. 2008;24(2):334-341. doi:10.1021/bp070301d
21. Pereira S, Kildegaard HF, Andersen MR. Impact of CHO metabolism on cell growth and protein production: an overview of toxic and inhibiting metabolites and nutrients. *Biotechnol J*. 2018;13(3):1700499. doi:10.1002/biot.201700499
22. Brunner M, Doppler P, Klein T, Herwig C, Fricke J. Elevated pCO_2 affects the lactate metabolic shift in CHO cell culture processes. *Eng Life Sci*. 2017;18(3):204-214. doi:10.1002/elsc.201700131
23. Xing Z, Li Z, Chow V, Lee SS. Identifying inhibitory threshold values of repressing metabolites in CHO cell culture using multivariate analysis Methods. *Biotechnol Prog*. 2008;24(3):675-683. doi:10.1021/bp070466m
24. Lao MS, Toth D. Effects of ammonium and lactate on growth and metabolism of a recombinant Chinese hamster ovary cell culture. *Biotechnol Prog*. 1997;13(5):688-691. doi:10.1021/bp9602360
25. Alberts B. *Molecular Biology of the Cell*. 7th ed. Garland Science Taylor & Francis; 2002.
26. Kimura R, Miller WM. Effects of elevated pCO_2 and/or osmolality on the growth and recombinant tPA production of CHO cells. *Biotechnol Bioeng*. 1996;52(1):152-160. doi:10.1002/(sici)1097-0290(19961005)52:13.0.co;2-q
27. Boron WF. *Intracellular pH Regulation*. Springer eBooks; 1987:39-51. doi:10.1007/978-1-4684-5404-8_3
28. Thorens B, Vassalli P. Chloroquine and ammonium chloride prevent terminal glycosylation of immunoglobulins in plasma cells without affecting secretion. *Nature*. 1986;321(6070):618-620. doi:10.1038/321618a0
29. Gray DR, Chen S, Howarth W, Inlow D, Maiorella BL. CO_2 in large-scale and high-density CHO cell perfusion culture. *Cytotechnology*. 1996;22(1–3):65-78. doi:10.1007/bf00353925
30. Leblanc Y, Ramon C, Bihoreau N, Chevreux G. Charge variants characterization of a monoclonal antibody by ion exchange chromatography coupled on-line to native mass spectrometry: case study after a long-term storage at +5°C. *J Chromatogr B*. 2017;1048:130-139. doi:10.1016/j.jchromb.2017.02.017
31. Dakshinamurthy P, Mukunda P, Prasad Kodaganti B, et al. Charge variant analysis of proposed biosimilar to trastuzumab. *Biologicals*. 2017;46:46-56. doi:10.1016/j.biologicals.2016.12.006
32. Rehder DS, Chelius D, McAuley A, et al. Isomerization of a single aspartyl residue of anti-epidermal growth factor receptor immunoglobulin γ2 antibody highlights the role avidity plays in antibody activity. *Biochemistry*. 2008;47(8):2518-2530. doi:10.1021/bi7018223
33. Antes B, Amon S, Rizzi A, et al. Analysis of lysine clipping of a humanized Lewis-Y specific IgG antibody and its relation to fc-mediated effector function. *J Chromatogr B*. 2007;852(1–2):250-256. doi:10.1016/j.jchromb.2007.01.024
34. Lyubarskaya Y, Houde D, Woodard J, Murphy D, Mhatre R. Analysis of recombinant monoclonal antibody isoforms by electrospray ionization mass spectrometry as a strategy for streamlining characterization of recombinant monoclonal antibody charge heterogeneity. *Anal Biochem*. 2006;348(1):24-39. doi:10.1016/j.ab.2005.10.003
35. Manning MC, Chou DK, Murphy BM, Payne RW, Katayama DS. Stability of protein pharmaceuticals: an update. *Pharm Res*. 2010;27(4):544-575. doi:10.1007/s11095-009-0045-6
36. Thomann M, Reckermann K, Reusch D, Prasser J, Tejada ML. Fc-galactosylation modulates antibody-dependent cellular cytotoxicity of therapeutic antibodies. *Mol Immunol*. 2016;73:69-75. doi:10.1016/j.molimm.2016.03.002
37. Musolino A, Naldi N, Bortesi B, et al. Immunoglobulin G fragment C receptor polymorphisms and clinical efficacy of trastuzumab-based therapy in patients with HER-2/*neu*–positive metastatic breast cancer. *J Clin Oncol*. 2008;26(11):1789-1796. doi:10.1200/jco.2007.14.8957
38. Chan KF, Goh JS, Song Z. Improving sialylation of recombinant biologics for enhanced therapeutic efficacy. *Pharm Bioprocess*. 2014;2(5):363-366. doi:10.4155/pbp.14.44
39. Bas M, Terrier A, Jacque E, et al. Fc sialylation prolongs serum half-life of therapeutic antibodies. *J Immunol*. 2019;202(5):1582-1594. doi:10.4049/jimmunol.1800896
40. Umaña P, Jean–Mairet J, Moudry R, Amstutz H, Bailey JE. Engineered glycoforms of an antineuroblastoma IgG1 with optimized antibody-dependent cellular cytotoxic activity. *Nat Biotechnol*. 1999;17(2):176-180. doi:10.1038/6179
41. Shields RL, Lai J, Keck R, et al. Lack of fucose on human IgG1N-linked oligosaccharide improves binding to human FcγRIII and antibody-dependent cellular toxicity. *J Biol Chem*. 2002;277(30):26733-26740. doi:10.1074/jbc.m202069200
42. Shinkawa T, Nakamura K, Yamane N, et al. The absence of fucose but not the presence of galactose or BisectingN-acetylglucosamine of human IgG1 complex-type oligosaccharides shows the critical role of enhancing antibody-dependent cellular cytotoxicity. *J Biol Chem*. 2002;278(5):3466-3473. doi:10.1074/jbc.m210665200
43. Majewska NI, Tejada ML, Betenbaugh MJ, Agarwal N. N-glycosylation of IgG and IgG-like recombinant therapeutic proteins: why is it important and how can we control it? *Annu Rev Chem Biomol Eng*. 2020;11(1):311-338. doi:10.1146/annurev-chembioeng-102419-010001
44. Chitwood DG, Wang Q, Klaubert SR, et al. Microevolutionary dynamics of eccDNA in Chinese hamster ovary cells grown in fed-batch cultures under control and lactate-stressed conditions. *Sci Rep*. 2023;13(1):1200. doi:10.1038/s41598-023-27962-0

SUPPORTING INFORMATION

Additional supporting information can be found online in the Supporting Information section at the end of this article.

How to cite this article: Klaubert SR, Chitwood DG, Peng D, et al. Dynamic pH profiles drive higher cell-specific and volumetric productivity. *Biotechnol. Prog*. 2025;e70080. doi:10.1002/btpr.70080